



HAL
open science

Reciprocal regulation of Aurora kinase A and ATIP3 in the control of metaphase spindle length

Anne Nehlig, Cynthia Seiler, Yulia Steblyanko, Florent Dingli, Guillaume Arras, Damarys Loew, Julie Welburn, Claude Prigent, Marin Barisic, Clara Nahmias

► **To cite this version:**

Anne Nehlig, Cynthia Seiler, Yulia Steblyanko, Florent Dingli, Guillaume Arras, et al.. Reciprocal regulation of Aurora kinase A and ATIP3 in the control of metaphase spindle length. Cellular and Molecular Life Sciences, 2021, 78 (4), pp.1765-1779. 10.1007/s00018-020-03614-8 . hal-02924786

HAL Id: hal-02924786

<https://hal.science/hal-02924786>

Submitted on 31 Aug 2020

HAL is a multi-disciplinary open access archive for the deposit and dissemination of scientific research documents, whether they are published or not. The documents may come from teaching and research institutions in France or abroad, or from public or private research centers.

L'archive ouverte pluridisciplinaire **HAL**, est destinée au dépôt et à la diffusion de documents scientifiques de niveau recherche, publiés ou non, émanant des établissements d'enseignement et de recherche français ou étrangers, des laboratoires publics ou privés.



Reciprocal regulation of Aurora kinase A and ATIP3 in the control of metaphase spindle length

Anne Nehlig^{1,2,3} · Cynthia Seiler^{1,2,3} · Yulia Steblyanko⁴ · Florent Dingli⁵ · Guillaume Arras⁵ · Damarys Loew⁵ · Julie Welburn⁶ · Claude Prigent⁷ · Marin Barisic^{4,8} · Clara Nahmias^{1,2,3}

Received: 30 January 2020 / Revised: 18 July 2020 / Accepted: 7 August 2020
© Springer Nature Switzerland AG 2020

Abstract

Maintaining the integrity of the mitotic spindle in metaphase is essential to ensure normal cell division. We show here that depletion of microtubule-associated protein ATIP3 reduces metaphase spindle length. Mass spectrometry analyses identified the microtubule minus-end depolymerizing kinesin Kif2A as an ATIP3 binding protein. We show that ATIP3 controls metaphase spindle length by interacting with Kif2A and its partner Dda3 in an Aurora kinase A-dependent manner. In the absence of ATIP3, Kif2A and Dda3 accumulate at spindle poles, which is consistent with reduced poleward microtubule flux and shortening of the spindle. ATIP3 silencing also limits Aurora A localization to the poles. Transfection of GFP-Aurora A, but not kinase-dead mutant, rescues the phenotype, indicating that ATIP3 maintains Aurora A activity on the poles to control Kif2A targeting and spindle size. Collectively, these data emphasize the pivotal role of Aurora kinase A and its mutual regulation with ATIP3 in controlling spindle length.

Keywords Aurora A · Dda3 · Kif2A · *MTUS1* · Mitotic kinase · Mitotic spindle · Poleward microtubule flux

Introduction

The size of the mitotic spindle in metaphase varies among different cell types and species but remains constant for a given cell type, despite high dynamics of spindle microtubules [1–3]. The spindle in metaphase must reach an optimal size to capture and bi-orient all duplicated chromosomes prior to cell division, and to allow separation of

the asters beyond a minimal distance for proper cleavage by the cytokinesis machinery at late stages of cell division [3]. Defects in spindle size and architecture can lead to mitotic defects and promote aneuploidy, which is a hallmark of cancer. Metaphase spindle length is controlled by intrinsic and extrinsic factors [3]. Poleward microtubule flux, which consists of translocation of tubulin heterodimers towards the poles, coupled to a balance between polymerization of microtubule plus ends at kinetochores and depolymerization of minus ends at the poles [4, 5], is a major mechanism to maintain the spindle at a constant

Electronic supplementary material The online version of this article (<https://doi.org/10.1007/s00018-020-03614-8>) contains supplementary material, which is available to authorized users.

✉ Clara Nahmias
clara.nahmias@inserm.fr

¹ Inserm U981, Department of Molecular Medicine, Gustave Roussy Cancer Center, Institut Gustave Roussy, 114 rue Edouard Vaillant, 94800 Villejuif, France

² LabEx LERMIT, Université Paris Saclay, 92296 Châtenay-Malabry, France

³ Institut Gustave Roussy, Inserm, Biomarqueurs prédictifs et nouvelles stratégies thérapeutiques en oncologie, Université Paris-Saclay, 94800 Villejuif, France

⁴ Cell Division Laboratory, Danish Cancer Society Research Center, 2100 Copenhagen, Denmark

⁵ Centre de Recherche, Laboratoire de Spectrométrie de Masse Protéomique, Institut Curie, PSL Research University, 75248 Paris Cedex 05, France

⁶ Wellcome Trust Centre for Cell Biology, School of Biological Sciences, University of Edinburgh, Edinburgh, Scotland, UK

⁷ Institut de Génétique et Développement de Rennes (IGDR), Unité CNRS, UMR 6290, Université de Rennes, 35043 Rennes, France

⁸ Department of Cellular and Molecular Medicine, Faculty of Health Sciences, University of Copenhagen, 2100 Copenhagen, Denmark

length in metaphase [2, 6]. Microtubule-associated proteins and depolymerizing kinesins, that regulate microtubule dynamics at both ends, thus appear as important regulators of poleward flux and spindle length [3, 7–9].

The Kif2A kinesin is a key regulator of poleward microtubule flux and spindle size in drosophila, xenopus and human cells [6, 10–13]. Kif2A belongs to the kinesin-13 family of depolymerizing kinesins also including Kif2B and MCAK/Kif2C [14]. During mitosis, Kif2A localizes to spindle poles where it depolymerizes microtubule minus ends [10, 15, 16], thereby controlling the rate of poleward microtubule flux. Transport of Kif2A to spindle poles is ensured by minus-end-directed motor protein dynein/dynactin [10] and is increased by interaction with microtubule-associated Dda3 protein, whose expression and phosphorylation are markedly elevated in mitosis [17, 18]. Depletion of either Dda3 or Kif2A increases mitotic spindle size [10, 17]. The microtubule depolymerizing activity of Kif2A and its recruitment to the poles are inhibited by Aurora kinase A (Aurora A) [19], a major mitotic kinase that localizes on spindle poles. Aurora A fulfills numerous functions [20, 21] including the regulation of spindle size [13, 22]. However, the mechanisms by which this kinase controls metaphase spindle length are poorly defined. Whether the maintenance of correct spindle size in metaphase depends on Aurora A-mediated regulation of Kif2A recruitment to the poles remains to be investigated.

ATIP3 is a microtubule-associated protein that decorates the centrosome and microtubule cytoskeleton in interphase, and the mitotic spindle and spindle poles during mitosis [23]. Previous studies have shown that ATIP3 is a potent microtubule stabilizer [24] that reduces microtubule dynamics by interacting with End-Binding protein EB1 in interphase [25, 26]. ATIP3 is the product of candidate tumor suppressor gene *MTUS1* whose expression is markedly down-regulated in aggressive breast tumors [23, 24]. We have recently shown that ATIP3 depletion is associated with increased aneuploidy and mitotic defects [27].

In this study, we show that ATIP3 depletion leads to shortening of the metaphase spindle. Mass spectrometry analysis identified Kif2A as an intracellular partner of ATIP3. We provide evidence that ATIP3 forms a complex with Kif2A and Dda3 and limits their recruitment to the poles, thereby contributing to maintaining constant spindle size in metaphase. The interaction between ATIP3, Dda3 and Kif2A is increased in mitosis and requires phosphorylation by Aurora kinase A. Conversely, the localization of Aurora A at spindle poles is regulated by ATIP3. Overall, we show that reciprocal regulation of ATIP3 and Aurora kinase A during mitosis ensures the timely assembly of a molecular ATIP3-Dda3-Kif2A complex that controls metaphase spindle length.

Materials and methods

Cell lines and synchronization

Human cancer cell lines MCF-7, MCF-7 cells stably expressing moderate levels of GFP-ATIP3 (HC6 clone), HCC1143 and HeLa were described previously [23, 24]. MCF-7 cells express undetectable levels of ATIP3 whereas HCC1143 and HeLa cells express endogenous ATIP3 [23, 24]. MCF-7 cells were cultured in DMEM-F12 supplemented with 5% bovine calf serum. HCC1143 cells were cultured in RMPI supplemented with 10% bovine calf serum and 1% sodium pyruvate. HeLa cells were cultured in DMEM supplemented with 10% bovine calf serum, 100 U/ml penicillin, and 100 U/ml streptomycin (all from Gibco) at 37 °C and 5% CO₂. Cells were routinely authenticated by morphologic observation and tested for absence of mycoplasma contamination using Venor[®] GeM Advance Kit (MB Minerva biolabs[®]).

For synchronization in metaphase, MCF-7 and HCC1143 cells were treated with 50 ng/ml nocodazole for 16 h and released for 45 min.

Plasmid constructs, siRNAs and transfections

Plasmids encoding GFP-ATIP3, GFP-D1, GFP-D2, GFP-D2, GFP-D2N, GFP-D2C, GFP-D3, GFP-ATIP3delCN and GFP-D2delCN were described elsewhere [24, 25]. Deletion mutants GFP-delCN2 and GFP-D2delCN2 (lacking amino acid positions 635–816 of ATIP3, accession number NP_001001924) were obtained by PCR amplification of the ATIP3 and D2 sequence, respectively, using the following oligonucleotides: 5'-GGG TCC GTT TCT GCG TTG TTT TCT GGT AAT GCC GCT GTC-3' and 5'-GAC AGC GGC ATT ACC AGA AAA CAA CGC AGA AAC GGA CCC-3' and QuikChange[®] II XL Site-Directed and Mutagenesis Kit (Agilent). Plasmids encoding GFP-AurA and GFP-AurA-KD were described elsewhere [28–30]. Plasmid encoding Kif2A-GFP was provided by Jamel Chelly (Institut de Génétique et de Biologie Moléculaire et Cellulaire, Strasbourg, France). All cDNA constructs were transfected (2–4 µg) for 24 h using X-treme Gene 9 (Roche) or Lipofectamine 2000 (Invitrogen) and were expressed at levels similar to those of endogenous proteins.

Specific and control scrambled siRNAs were from Dharmacon (ThermoFisher Scientific). The following sequences were used: ATIP3#1, 5'-UGGCAGAGUUU AAG GUUA-3'; ATIP3#2, 5'-GCAAUAGCUGCUCC AAAA-3'; Kif2A, 5'-GGCAAAGAGAUUG ACCUGG-3'; Aurora A, 5'-AUGCCCUGUCUACUGUCA-3'; Dda3, 5'-AAGCAAGACU UCAGUAGCAUU-3'. For rescue

136 experiments of ATIP3 knock-down, HeLa cells were trans- 185
 137 fected with ATIP3#1 siRNA that targets the 5' untranslated 186
 138 sequence of ATIP3 and allows ectopic expression of the 187
 139 ATIP3 coding sequence [25]. 188

140 All siRNAs (50 nM) were transfected for 48–72 h using 189
 141 Lipofectamine 2000 (Invitrogen) and silencing efficiency 190
 142 was evaluated by immunoblotting. Antibodies used for 191
 143 immunoblotting were rabbit anti-ATIP3 (anti-MTUS1; 192
 144 ARP44419-P050; Aviva Systems, 1/1000e), rabbit anti- 193
 145 Kif2A (ab37005; Abcam, 1/5000e), mouse anti-Aurora A 194
 146 (ab13824; Abcam, 1/1000e), rabbit anti-Dda3 (GTX128047; 195
 147 GeneTex, 1/1000e), rabbit anti-GFP (6556; Abcam, 196
 148 1/1000e), mouse anti-GFP (ab1218; Abcam, 1/1000e), 197
 149 mouse anti-alpha-tubulin (T9026; Abcam, 1/5000e), anti- 198
 150 phospho-histone H3 (06-570; Millipore, 1/1000e), mouse 199
 151 anti-gamma-actin (ab123034; Abcam, 1/5000e), mouse anti- 200
 152 vinculin (V9264; Sigma, 1/5000e). 201

153 Immunoprecipitations 202

154 HeLa or MCF-7 cells were transfected as described above 203
 155 and lysed in lysis buffer containing 50 mM Tris-HCl pH 204
 156 7.4, 150 mM NaCl, 1 mM EDTA, 2.5 mM MgCl₂, 0.2 M 205
 157 PMSF, 1 mM Aprotinin, 5 mg/ml Leupeptin, 2 mg/ml 206
 158 Pepstatin, 0.2 M orthovanadate, 1 M sodium fluoride, and 207
 159 10 μM okadaic acid. Lysates were centrifuged, incubated 208
 160 with uncoupled magnetic agarose beads at 4 °C for 15 min, 209
 161 and then incubated with anti-GFP VHH coupled to magnetic 210
 162 agarose beads (GFP-trap_MA; Chromotek) at 4 °C over- 211
 163 night. Antibody beads were recovered with a bar magnet, 212
 164 washed once with the lysis buffer in the presence of anti- 213
 165 proteases and then twice with the lysis buffer, and analyzed 214
 166 by Western blotting with appropriate antibodies as described 215
 167 above. Results shown are representative of 3–5 independent 216
 168 experiments. 217

169 Proteomics and mass spectrometry 218

170 MCF-7 cells were transiently transfected with 2 μg of GFP- 219
 171 ATIP3 or GFP for 24 h then lysed as described above. For 220
 172 immuno-isolated samples, 1 mg extract was incubated with 221
 173 25 μl magnetic beads (GFP-trap_MA; Chromotek) for 2 h 222
 174 at 4 °C. 223

175 Proteins on magnetic beads were washed twice with 224
 176 100 μl of 25 mM NH₄HCO₃ and on-beads digestion were 225
 177 performed with 0.2 μg of trypsin/LysC (Promega) for 1 h 226
 178 in 100 μl of 25 mM NH₄HCO₃. Sample were then loaded 227
 179 onto a homemade C18 StageTips for desalting (principle by 228
 180 stacking one 3 M Empore SPE Extraction Disk Octadecyl 229
 181 (C18) and beads from SepPak C18 Cartridge Waters into a 230
 182 200 μl micropipette tip). Peptides were eluted using 40/60 231
 183 MeCN/H₂O + 0.1% formic acid and vacuum concentrated 232
 184 to dryness. 233

Online chromatography was performed with an RSLC- 234
 nano system (Ultimate 3000, Thermo Scientific) coupled 235
 online to an Orbitrap Fusion Tribrid mass spectrometer
 (Thermo Scientific). Peptides were trapped on a C18 col-
 umn (75 μm inner diameter × 2 cm; nanoViper Acclaim
 PepMapTM 100, Thermo Scientific) with buffer A (2/98
 MeCN/H₂O in 0.1% formic acid) at a flow rate of 4.0 μl/min
 over 4 min. Separation was performed on a 50 cm × 75 μm
 C18 column (nanoViper Acclaim PepMapTM RSLC,
 2 μm, 100 Å, Thermo Scientific) regulated to a temperature
 of 55 °C with a linear gradient of 2–30% buffer B (100%
 MeCN in 0.1% formic acid) at a flow rate of 350 nl/min over
 160 min. Full-scan MS was acquired in the Orbitrap analyzer
 with a resolution set to 120,000 and ions from each full scan
 were HCD fragmented and analyzed in the linear ion trap.

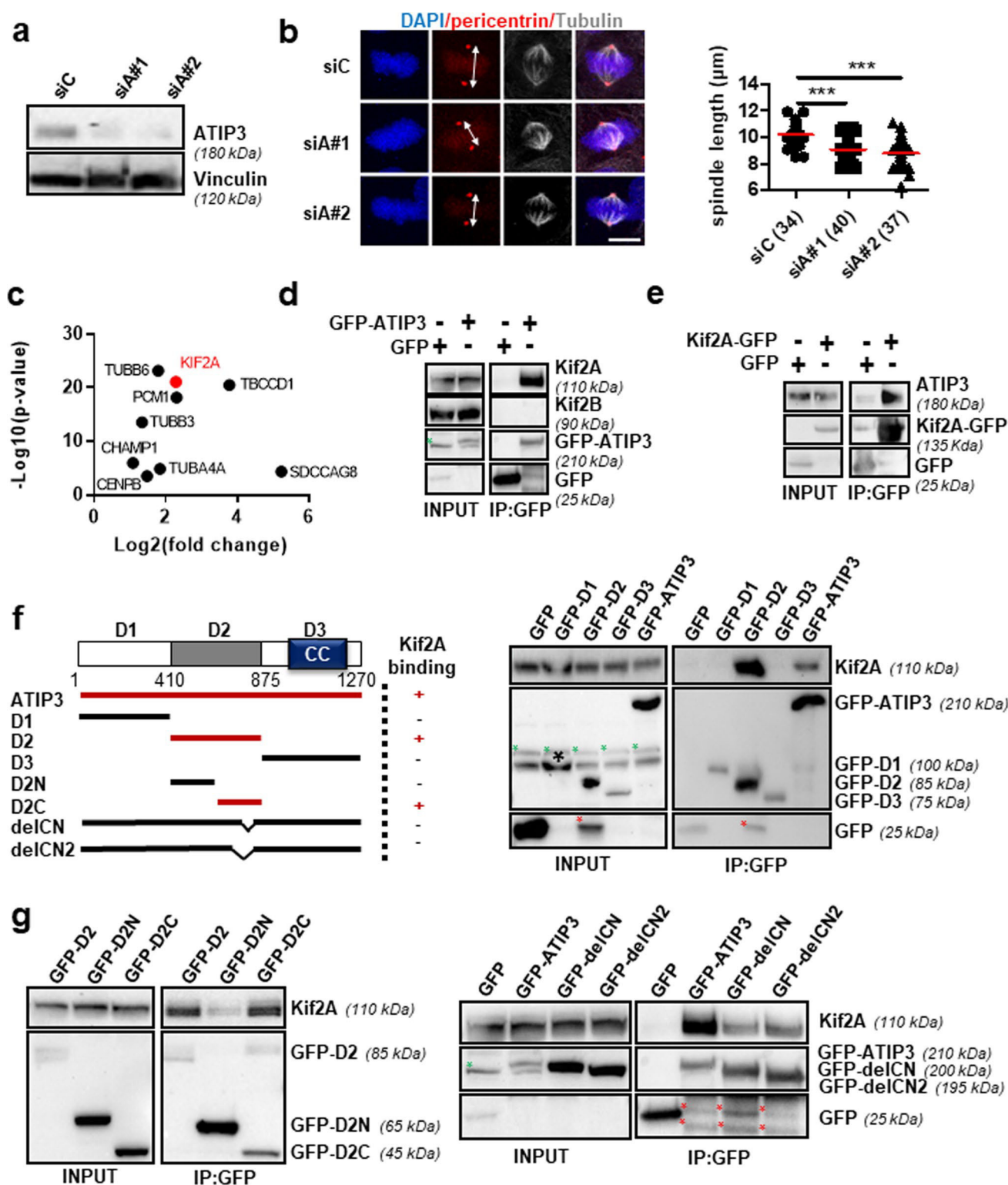
For identification the data were searched against the Swis-
 sProt Homo Sapiens (February 2017, no isoforms) database
 using Sequest HF through proteome discoverer (version 2.1).
 Enzyme specificity was set to trypsin and a maximum of two
 missed cleavage site were allowed. Oxidized methionine,
 N-terminal acetylation, and carbamidomethyl cysteine were
 set as variable modifications. Maximum allowed mass devia-
 tion was set to 10 ppm for monoisotopic precursor ions and
 0.6 Da for MS/MS peaks.

The resulting files were further processed using myProMS
 [31] v3.6 (work in progress). FDR calculation used Perc-
 olator and was set to 1% at the peptide level for the whole
 study. The label free quantification was performed by pep-
 tide Extracted Ion Chromatograms (XICs) computed with
 MassChroQ version 2.2.2 [32]. For protein quantification,
 XICs from proteotypic peptides shared between compared
 conditions (TopN matching) with no missed cleavages were
 used. Median and scale normalization was applied on the
 total signal to correct the XICs for each biological replicate.
 To estimate the significance of the change in protein abun-
 dance, a linear model (adjusted on peptides and biological
 replicates) was performed and *p*-values were adjusted with a
 Benjamini–Hochberg FDR procedure with a control thresh-
 old set to 0.05. Fold change-based GO enrichment analysis
 was performed as described [33].

The mass spectrometry proteomics data have been
 deposited to the ProteomeXchange Consortium via the
 PRIDE [34] partner repository with the dataset identifier
 PXD009182 (username: reviewer03478@ebi.ac.uk, pass-
 word: UFFpYuYZ).

230 Immunofluorescence 230

231 Cells were fixed on cover glasses with ice-cold methanol for
 232 5 min and washed with PBS. Coverslips were subsequently
 233 incubated at room temperature for 1 h in primary antibodies
 234 and for 1 h in Alexa Fluor 488-, Alexa Fluor 549- and Alexa
 235 Fluor 647-coupled secondary antibodies diluted in PBS/



236 Triton 0.1%, BSA 0.2%. The following primary antibodies were used: rabbit anti-Kif2A (ab37005; Abcam, 1/250e),
 237 rabbit anti-pericentrin (ab4448; Abcam, 1/500e), rabbit anti-Dda3 (GTX128047; GeneTex, 1/500e), mouse anti-Aurora
 238 A (ab13824; Abcam, 1/200e), rabbit Phospho-Aurora A

(Thr288) (3079S; Cell Signaling, 1/200e), mouse anti-GFP (ab1218; Abcam, 1/250e), rat anti-alpha-tubulin (ab6160; Abcam, 1/500e), mouse anti-gamma-tubulin (T5326; Sigma, 1/500e) and mouse anti-alpha-tubulin (T9026; Sigma, 1/100e). Coverslips were fixed with Glycergel Mounting

241
242
243
244
245

Fig. 1 ATIP3 interacts with Kif2A. **a** Immunoblotting with anti-ATIP3 (MTUS1) antibodies shows silencing efficiency of two different ATIP3-specific siRNAs (siA#1 and siA#2) transfected in HeLa cells. Blots were reprobated with anti-vinculin antibodies for internal control. **b** Immunofluorescence imaging of HeLa cells transfected with control (siC), and two different ATIP3-specific siRNAs (siA#1 and siA#2) as indicated. Cells were stained with anti-pericentrin (red), anti-alpha-tubulin (gray) antibodies and DAPI (blue). Scale bar, 10 μ m. Pole-to pole distance (white arrow) was measured by drawing a line with ImageJ software between the two poles stained with pericentrin. Right panel shows quantification of spindle length in metaphase. Number of cells analyzed is under brackets. *** $p < 0.001$. **c** Volcano plot showing distribution of the 9 proteins related to the microtubule cytoskeleton and/or mitosis present in GFP-ATIP3 compared with GFP and identified by mass spectrometry. x axis = $\log_2(\text{fold-change})$, y axis = $-\log_{10}(p\text{-value})$. Position of the ATIP3 partner Kif2A is indicated in red. **d** MCF-7 cells were transfected with GFP-ATIP3 or GFP and immunoprecipitation was performed using anti-GFP antibodies. Western blots were probed with anti-Kif2A, Kif2B, anti-ATIP3 and anti-GFP antibodies to reveal Kif2A, Kif2B, GFP-ATIP3 and GFP, respectively. A green asterisk in the INPUT panel indicates endogenous ATIP3. **e** HeLa cells were transfected with Kif2A-GFP or GFP and immunoprecipitation was performed using anti-GFP antibodies. Western blots were probed with anti-ATIP3 (MTUS1) and anti-GFP antibodies to reveal ATIP3, Kif2A-GFP and GFP. **f** Schematic representation of the ATIP3 protein sequence illustrating the position of D1, D2 and D3 regions and ATIP3 deletion mutants and their ability (+) or not (-) to bind Kif2A. Kif2A-binding regions are in red. CC: coiled coil region. Amino acid numbering is from accession number NP_001001924. Right panel: immunoprecipitation assay of MCF-7 cell lysates expressing GFP, GFP-ATIP3 or GFP-fused D1, D2, D3 regions. Blots were probed with anti-Kif2A and anti-GFP antibodies. A green asterisk indicates non-specific band. A black star indicates the position of GFP-D1 which migrates at the same apparent molecular weight as endogenous Kif2A revealed in previous blotting. A red asterisk indicates cleavage product of GFP-D2. **g** MCF-7 cells were transfected with GFP-D2 fragments (left panel) or GFP-ATIP3 deletion mutants (right panel) and immunoprecipitation was performed using anti-GFP antibodies. Blots were probed as in **d**. A green asterisk shows endogenous ATIP3. Red asterisks indicate cleavage products of fusion proteins

246 Medium (Dako) coupled with DAPI. Images were acquired
247 with a confocal laser scanning microscope Dmi8- SP8 with
248 an HC PL APO CS2 40x-1.3 Oil (Leica). Linescan analyses
249 of pole-to-pole distance and fluorescence intensities were
250 done with Image J. At least 30 cells in 4–10 fields per condi-
251 tion were analyzed.

252 Results shown are representative of 3–5 independent
253 experiments.

254 Fluorescence recovery after photobleaching (FRAP)

255 HeLa cells were transfected with control or ATIP3 siRNA
256 and co-transfected with Kif2A-GFP. For the experi-
257 ment, cells were seeded in 35 mm glass-bottomed dishes
258 (14 mm, No. 1.5, MatTek Corporation). The siRNA trans-
259 fection was done 72 h prior to filming using Lipofectamine
260 2000 (Invitrogen). Kif2A-GFP was co-transfected 48 h
261 after siRNA transfection. 10 nM SiR-DNA (Spirochrome)

262 was added to the cell culture medium 30 min before start-
263 ing the live-cell imaging. Time-lapse imaging was per-
264 formed at 37 °C using a Plan-Apochromat 63x/1.4NA with
265 differential interference contrast oil objective mounted on
266 an inverted Zeiss Axio Observer Z1 microscope (Marianas
267 Imaging Workstation from Intelligent Imaging and
268 Innovations Inc. (3i), Denver, CO, USA), equipped with a
269 CSU-X1 spinning-disk confocal head (Yokogawa Corpo-
270 ration of America). Images were acquired using an iXon
271 Ultra 888 EM-CCD camera (Andor Technology). After
272 identification of spindle poles in metaphase cells, one of
273 the two poles was photobleached with a 5 ms laser pulse
274 using 100% power of the 488 nm solid state laser, and
275 the fluorescence recovery was recorded for 90 s at 500 ms
276 intervals. For FRAP calculations, the fluorescence inten-
277 sity of the bleached area was normalized using the inten-
278 sity of the whole cell, after background correction. Then
279 a full-scale normalization was performed and the mean
280 values were plotted and used for exponential curve fitting
281 using GraphPad Prism 7.01 to determine the half-life and
282 efficiency of the recovery.

283 Poleward microtubule flux rate measurement

284 Photo-conversion of alpha-tubulin was performed using
285 a stable U2OS-mEOS-tubulin cell line [35] cultivated on
286 35 mm glass-bottomed dishes (14 mm, No. 1.5, MatTek
287 Corporation). Transfection of control or ATIP3 siRNA
288 was done 48 h prior to filming using Lipofectamine 2000
289 (Invitrogen). Time-lapse imaging was performed at 37 °C
290 using a Plan-Apochromat 63x/1.4NA oil objective with
291 differential interference contrast mounted on an inverted
292 Zeiss Axio Observer Z1 microscope (Marianas Imaging
293 Workstation from Intelligent Imaging and Innovations
294 Inc. (3i), Denver, CO, USA), equipped with a CSU-X1
295 spinning-disk confocal head (Yokogawa Corporation of
296 America) and a photo-activation system with 405 nm laser
297 line. Images were acquired using an iXon Ultra 888 EM-
298 CCD camera (Andor Technology). Late prometaphase/
299 metaphase cells were identified upon green fluorescent
300 tubulin signals and two line-shaped regions of interest
301 were placed perpendicular to the main spindle axis on
302 both sides of the metaphase plate to be photo-activated.
303 Photo-conversion was performed by a 5-ms 405-nm laser
304 pulse. Photo-converted red signals were then followed over
305 time together with green fluorescence signal using 561-
306 and 488-nm lasers and images were acquired every 5 s for
307 3 min. Microtubule flux was quantified by tracking photo-
308 converted mEos-tubulin over time using sum-projected
309 kymographs generated by a MATLAB-based algorithm
310 [36].

311 Statistical analysis

312 Statistical analyses were done using GraphPad Prism 6.0
313 software. Data in bar graphs (mean \pm SD) and dot plots were
314 analyzed using two-tail unpaired *t* test and ANOVA test.
315 $p < 0.05$ was considered statistically significant.

316 Results

317 ATIP3 depletion reduces metaphase spindle length

318 To evaluate the consequences of ATIP3 depletion in mitosis,
319 HeLa cells were transfected with two independent
320 ATIP3 siRNAs (siA#1 and siA#2) (Fig. 1a) and mitotic
321 cells were analyzed by immunofluorescence. By measuring
322 pole-to-pole distance in metaphase cells using pericentrin
323 as a marker, we observed that ATIP3 depletion with each
324 siRNA reduces spindle length (Fig. 1b). Similar results were
325 obtained using both ATIP3 siRNAs in HCC1143 breast
326 cancer cells (Fig. S1A). Conversely, moderate expression
327 of GFP-ATIP3 in ATIP3-negative MCF-7 cells led to an
328 increase in spindle size compared to control cells expressing
329 GFP (Fig. S1B).

330 Other mitotic defects such as multipolar spindles
331 (Fig. S1C) and spindle mispositioning (Fig. S1D) were
332 observed in ATIP3-depleted cells but spindle orientation,
333 symmetry and cell size remained unchanged (Fig. S1E).

334 ATIP3 interacts with Kif2A

335 In a first step to elucidate the molecular mechanisms
336 by which ATIP3 controls spindle size, we undertook a

337 proteomic approach to identify novel intracellular ATIP3
338 binding partners. Anti-GFP antibodies were used to immu-
339 noprecipitate molecular complexes from MCF-7 breast
340 cancer cells expressing either GFP or GFP-ATIP3 fusion
341 protein. Mass spectrometry analysis allowed us to identify
342 145 proteins that selectively interact with ATIP3 (Table S1),
343 nine of which were related to the microtubule cytoskeleton
344 and/or mitosis (Fig. 1c, Table 1). These include 3 tubulin
345 chains (beta6, alpha4 and beta3), 2 centromere/kinetochore
346 associated proteins (CENPB, CHAMP1) and 4 centrosomal/
347 spindle pole proteins (SDCCAG8, TBBCD1, PCM1
348 and Kif2A). The Kif2A kinesin was among the best candi-
349 date ATIP3 partners in terms of fold change (4.86) and
350 p value (8.14×10^{-22}). This depolymerizing kinesin is also
351 a well-known regulator of mitotic spindle length [10] and was
352 therefore selected for further studies.

353 The interaction between ATIP3 and Kif2A was con-
354 firmed by co-immunoprecipitation analyses. GFP-ATIP3
355 fusion protein expressed in MCF-7 cells was immuno-
356 precipitated using anti-GFP antibodies and found to bind
357 endogenous Kif2A (Fig. 1d). Kinesin Kif2B was not retained
358 in GFP-ATIP3 immunocomplexes, indicating specificity.
359 Conversely, endogenous ATIP3 was found to interact with
360 Kif2A-GFP in HeLa cells (Fig. 1e), confirming the exist-
361 ence of ATIP3-Kif2A molecular complexes. As shown in
362 Fig. S1F, ATIP3 accumulates along the entire length of
363 the spindle, including the spindle poles where Kif2A is
364 localized.

365 To better characterize the interaction, we analyzed three
366 truncated constructs designated D1, D2 and D3 (Fig. 1f)
367 encompassing the N-terminal acidic region, the central
368 MT-binding domain and the C-terminal coiled-coil region
369 of ATIP3, respectively [24]. After transient transfection of

Table 1 ATIP3-interacting partners related to microtubule cytoskeleton and/or mitosis

Gene and synonyms	ATIP3/GFP			Description
	Ratio	Log2	<i>p</i> -value	
MTUS1	400.563902	8.6458886	4.2716E-51	Microtubule-associated tumor suppressor 1
SDCCAG8	37.6347222	5.23399242	4.7636E-05	Serologically defined colon cancer antigen 8
TBCCD1	13.6959029	3.77567248	3.2558E-21	TBCC domain-containing protein 1
PCM1	4.92790341	2.30097398	6.9899E-19	Pericentriolar material 1 protein
KIF2A	4.86820741	2.28339063	8.1438E-22	Kinesin-like protein KIF2A
CENPB	3.58061441	1.84020717	1.35E-05	Major centromere autoantigen B
TUBB6	3.45212501	1.78748471	6.9563E-24	Tubulin beta-6 chain
TUBA4A	2.78607967	1.47823652	0.00032993	Tubulin alpha-4A chain
TUBB3	2.53211069	1.34034047	2.8227E-14	Tubulin beta-3 chain
CHAMP1	2.12271217	1.08590876	1.0626E-06	Chromosome alignment-maintaining phosphoprotein 1

MCF-7 cells were transfected with GFP or GFP-ATIP3 and cell lysates were precipitated using GFP-trap magnetic agarose beads. Proteins retained in immunocomplexes were analyzed by quantitative label-free mass spectrometry analysis performed on four replicates. Shown are the fold changes of 9 proteins related to microtubules and/or mitosis that were selected among 145 proteins quantified by label-free quantitative analysis of GFP-ATIP3 versus GFP according to absolute fold change ≥ 2 , adjusted p -value of ratio significance ≤ 0.05 and more than 3 peptides. Proteins are listed by ratio order

370 GFP-tagged constructs followed by co-immunoprecipitation, 419
 371 results showed that the central region of 410 amino-acids 420
 372 (D2 region) interacts with Kif2A (Fig. 1f, right panel). Trun- 421
 373 cated mutants of the D2 region (D2N, D2C) were then ana- 422
 374 lyzed. The D2C sequence encompassing amino acid residues 423
 375 705–874 of ATIP3 was sufficient to bind Kif2A (Fig. 1g, 424
 376 left panel). Deletion of amino acids 705–816 (GFP-delCN) 425
 377 and 635–816 (GFP-delCN2) in the ATIP3 sequence led to a 426
 378 marked decrease in Kif2A interaction (Fig. 1g, right panel). 427
 379 Deleting the same sequences from the D2 polypeptide also 428
 380 impaired the interaction (Fig. S2A), therefore indicating that 429
 381 a minimal sequence of 112 amino acids (CN sequence) is 430
 382 required for ATIP3 interaction with Kif2A. 431

383 **ATIP3-Kif2A complex controls metaphase spindle** 432 384 **length** 433

385 To investigate the functional impact of ATIP3-Kif2A com- 434
 386 plex in the control of mitotic spindle length, we investi- 435
 387 gated whether GFP-ATIP3 construct and deletion mutants 436
 388 were able to rescue the ATIP3 depletion phenotype. RNAi- 437
 389 resistant GFP-ATIP3 expressed at moderate levels in ATIP3- 438
 390 depleted cells indeed restored a spindle size similar to that 439
 391 observed in control cells (Fig. 2a). In contrast, deletion 440
 392 mutants GFP-DelCN and GFP-DelCN2—that are unable to 441
 393 interact with Kif2A—failed to rescue the phenotype (Fig. 2a, 442
 394 S2B). Furthermore, expressing the Kif2A-interacting 443
 395 region D2 was sufficient to restore a correct spindle length 444
 396 in ATIP3-depleted cells whereas Kif2A-binding defective 445
 397 mutants D2delCN and D2delCN2 were not (Fig. S2C). 446
 398 Together these data strongly suggest that ATIP3 may control 447
 399 metaphase spindle size by interacting with Kif2A. 448

400 **ATIP3 depletion increases Kif2A targeting** 449 401 **to the spindle poles** 450

402 Immunofluorescence studies revealed that ATIP3 depletion 451
 403 markedly increases Kif2A fluorescence intensity at spindle 452
 404 poles (Fig. 2b) with no effect on the cytosolic pool of Kif2A 453
 405 (Fig. S2D). In contrast, ATIP3 depletion did not significantly 454
 406 modify fluorescence intensity of pericentrin, a major spindle 455
 407 pole protein (Fig. S2E). Expression of RNAi-resistant GFP- 456
 408 ATIP3 in ATIP3-depleted cells rescued the phenotype and 457
 409 decreased Kif2A intensity at the poles (Fig. 2c). Of note, 458
 410 ATIP3 silencing had no effect on total Kif2A protein levels 459
 411 detected by western blotting (Fig. 2b, left panel), suggesting 460
 412 that increased fluorescence intensity of Kif2A may reflect 461
 413 increased recruitment to the poles rather than increased 462
 414 expression of the protein. 463

415 We then evaluated whether increased Kif2A accumula- 464
 416 tion at spindle poles may contribute to the phenotype of 465
 417 ATIP3 deficiency. Silencing of Kif2A in ATIP3-depleted 466
 418 cells (Fig. S2F) indeed rescued the phenotype and restored 467
 468
 469

a correct spindle size (Fig. 2d), indicating that increased 419
 Kif2A recruitment to the poles is responsible for spindle 420
 length shortening in ATIP3-depleted cells. 421

422 It has been previously shown that Kif2A regulates meta- 423
 phase spindle length by controlling poleward microtubule 424
 flux via its microtubule depolymerizing activity at the spin- 425
 dle poles [6, 10, 11]. We reasoned that ATIP3 deficiency 426
 may disrupt the balance of microtubule dynamics in the 427
 spindle by allowing increased Kif2A depolymerizing activ- 428
 ity at the poles, resulting in decreased poleward flux and 429
 shorter spindle length. To address that question, microtu- 430
 bule flux rates were analyzed following ATIP3 silencing in 431
 metaphase U2OS cells stably expressing alpha-tubulin fused 432
 to the photo-convertible fluorescent protein mEos2 [35]. 433
 Results indicate that poleward microtubule flux is signifi- 434
 cantly decreased in ATIP3-depleted cells ($0.53 \pm 0.13 \mu\text{m}/$ 435
 min) compared to control cells ($0.67 \pm 0.08 \mu\text{m}/\text{min}$, 436
 $p < 0.0001$) (Fig. 2e), supporting the notion that ATIP3 may 437
 control spindle size by regulating the recruitment—and thus, 438
 the depolymerizing activity—of Kif2A to the poles. Col- 439
 lectively, these data indicate that ATIP3 controls metaphase 440
 spindle length by interacting with the Kif2A kinesin and 441
 reducing its recruitment to the poles. 442

442 **ATIP3-Kif2A interaction involves Dda3** 443

443 How does ATIP3 silencing increase Kif2A targeting at the 444
 spindle poles? We hypothesized that ATIP3 may sequester 445
 Kif2A in the cytosol and slower the exchange rate between 446
 spindle pole-associated Kif2A and a diffuse cytosolic pool 447
 of the protein. We thus explored the dynamic behavior of 448
 Kif2A turnover on spindle poles in the presence or absence 449
 of ATIP3. Fluorescence recovery after photobleaching 450
 (FRAP) experiments were performed on metaphase HeLa 451
 cells expressing endogenous ATIP3 and transfected with 452
 Kif2A-GFP. Bleaching was done on one of the two spindle 453
 poles. We found that in control cells, Kif2A-GFP association 454
 with spindle poles is dynamic. Ninety percent of the signal 455
 was recovered after photobleaching, with a half-recovery 456
 time of 11.6 s (Fig. 3a) which is faster than that (30.7 s) 457
 reported for NuMA, another major spindle pole-associated 458
 protein [37]. In ATIP3-depleted cells, Kif2A-GFP fluores- 459
 cence recovery parameters remained unchanged (half-recov- 460
 ery time of 11.62 s), ruling out the hypothesis that ATIP3 461
 depletion may modify the exchange rate between cytosolic 462
 and spindle pole-associated pools of Kif2A. 463

464 We then investigated whether ATIP3 may regulate 465
 Kif2A localization by a mechanism involving Dda3, a 466
 microtubule-associated protein known to interact with and 467
 increase Kif2A targeting to spindle poles [17]. As shown 468
 in Fig. 3b, Dda3 silencing in ATIP3-depleted cells rescued 469
 Kif2A fluorescence intensity at spindle poles, indicating 470
 that Dda3 contributes to the regulatory effects of ATIP3 471

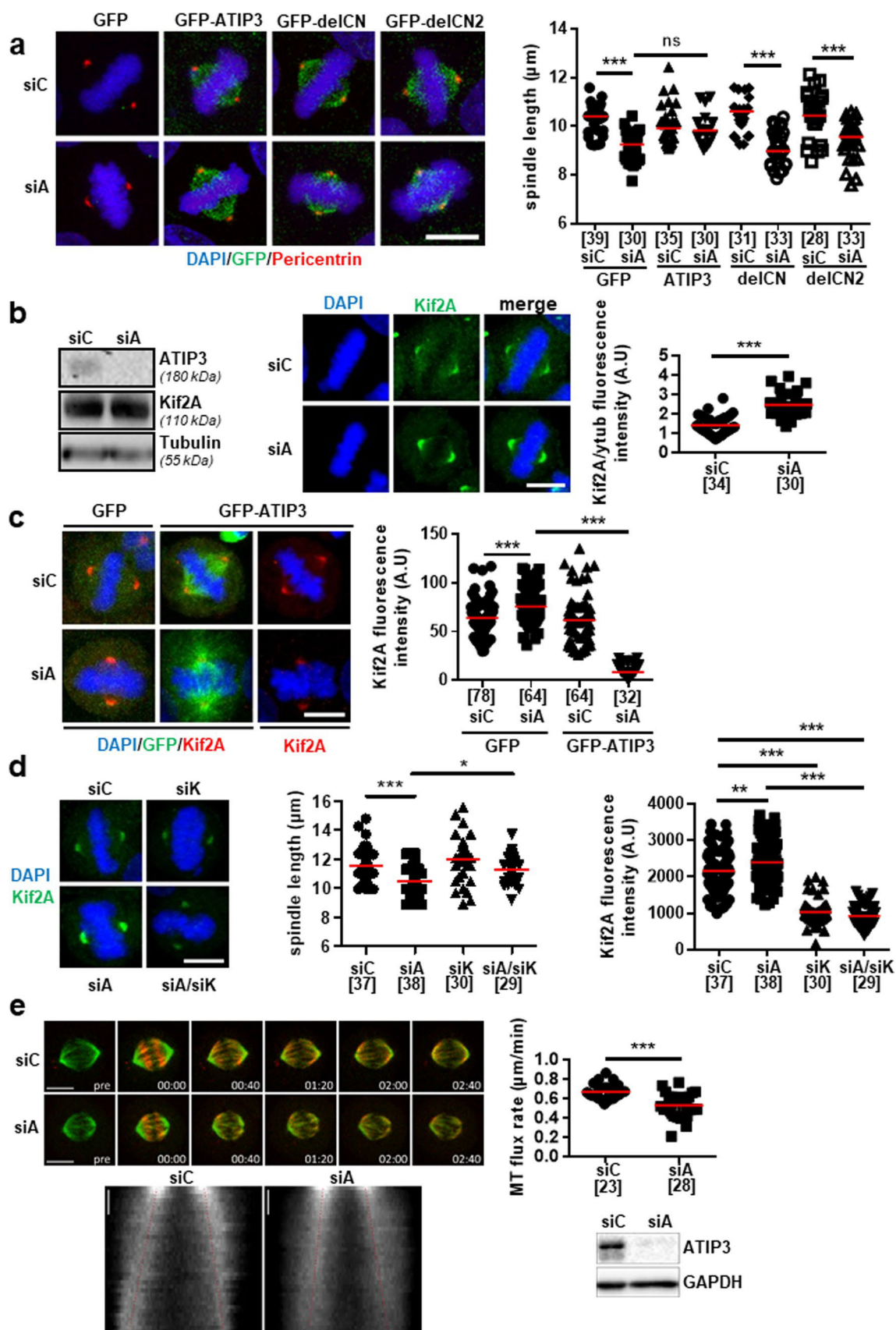


Fig. 2 ATIP3 regulates Kif2A recruitment to spindle poles. **a** Immunofluorescence imaging of HeLa cells transfected for 48 h with control (siC) or ATIP3-specific (siA) siRNA as indicated, then for 24 h with GFP, GFP-ATIP3, or ATIP3 deletion mutants (GFP-delCN and GFP-delCN2) as indicated. Cells were stained with anti-GFP (green) and anti-pericentrin (red) antibodies and DAPI (blue). Scale bar, 10 μ m. Spindle length was measured as in Fig. 1b. Right panel shows quantification of spindle length in metaphase HeLa cells. Number of cells analyzed is under brackets. *** $p < 0.001$, ns: not significant. **b** Left panel: Immunoblotting of HeLa cell lysates following transfection with control (siC) or ATIP3-specific (siA) siRNA as indicated. Blots were probed with anti-MTUS1 (ATIP3), anti-Kif2A and anti-tubulin antibodies. Middle panel: Immunofluorescence imaging of HeLa cells transfected with control (siC) or ATIP3-specific (siA) siRNA as indicated. Cells were fixed and stained with anti-Kif2A (green) antibodies and DAPI (blue). Scale bar, 10 μ m. Kif2A fluorescence intensity was measured by drawing a line with ImageJ software between the two poles and the maximum intensity values at the poles were collected and normalized to the intensity of gamma-tubulin. Right panel: Quantification of Kif2A intensity in metaphase HeLa cells. Number of poles analyzed is under brackets. *** $p < 0.001$. **c** Immunofluorescence imaging of HeLa cells transfected with control or ATIP3-specific siRNA for 48 h, then were transfected for 24 h with GFP or GFP-ATIP3, fixed and stained with anti-Kif2A (red) and anti-GFP (green) antibodies and DAPI (blue). Scale bar, 10 μ m. Right panel shows quantifications of Kif2A intensity at poles in metaphase HeLa cells. Number of poles analyzed is under brackets. *** $p < 0.001$. **d** Immunofluorescence imaging of HeLa cells transfected with control (siC), ATIP3-specific (siA) and/or Kif2A-specific (siK) siRNA as indicated, and stained as in **b**. Scale bar, 10 μ m. Middle panel: Spindle length (pole-to-pole distance) was measured as in Fig. 1b. Number of metaphase cells analyzed is under brackets. Right panel: Quantification of Kif2A intensity in metaphase HeLa cells as in **b**. Number of poles analyzed is under brackets. * $p < 0.05$, ** $p < 0.01$, *** $p < 0.001$. **e** Upper left panel: Representative fluorescence images of U2OS-mEOS-tubulin cells in late prometaphase/metaphase transfected with control (siC) and ATIP3 (siA) siRNAs. Images were captured before (pre) and after photo-conversion of mEOS-tubulin. Microtubule flux was measured by photoconversion of line-like regions from both half-spindles in mEOS-tubulin cells and tracking of photoconverted mEOS-tubulin over a time interval of 3 min. Scale bar, 10 μ m; time, min:s. Lower left panel: Representative sum-projected kymographs of photoactivated regions used for quantification of flux rates in control (siC) and ATIP3-depleted (siA) cells. Red dashed line indicates the slope of mEOS tubulin translocation over time. Scale bar, 30 s. Upper right panel: Quantification of microtubule flux in control versus ATIP3-depleted cells. Number of cells analyzed is under brackets. *** $p < 0.001$. Lower right panel: Immunoblotting-based validation of ATIP3 siRNA efficiency

470 on Kif2A recruitment. Accordingly, Dda3 silencing also
471 restored a correct spindle length in ATIP3-depleted cells
472 (Fig. 3b), indicating that Dda3 is essential to the ATIP3
473 phenotype. Immunofluorescence analyses revealed that,
474 as for Kif2A, Dda3 fluorescence intensity at the poles is
475 increased upon ATIP3 depletion (Fig. 3c). Conversely,
476 expression of GFP-ATIP3 led a decrease of Dda3 recruit-
477 ment to the poles compared with GFP (Fig. 3d). Of note,
478 silencing of either Kif2A or Dda3 had no significant effect
479 on ATIP3 fluorescence intensity (Fig. S3), pointing to
480 ATIP3 as an upstream regulator of Kif2A and Dda3 tar-
481 geting to the poles.

Dda3 is a known partner of Kif2A, raising the possibility
that it may be part of the ATIP3-Kif2A complex. Immu-
noprecipitation studies revealed that Dda3 indeed inter-
acts with ATIP3 (Fig. 3e). To evaluate whether Dda3 may
compete with, or contribute to, ATIP3-Kif2A interaction,
Dda3 was silenced using siRNA prior to immunoprecipita-
tion with GFP-ATIP3. Results showed that Dda3 depletion
impaired Kif2A binding to GFP-ATIP3 immunocomplexes
(Fig. 3f) indicating that Dda3 is required for ATIP3-Kif2A
interaction.

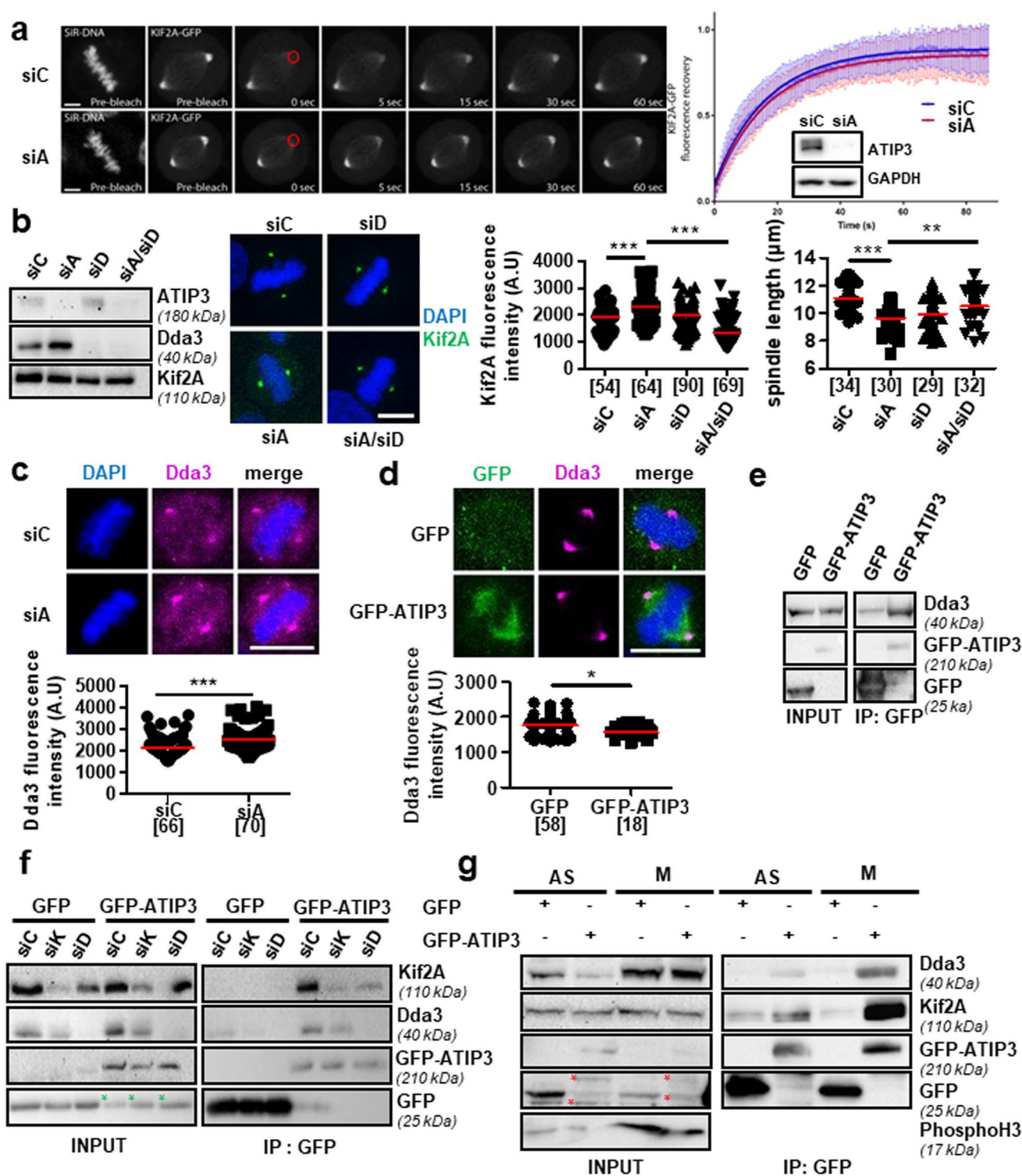
The interaction between ATIP3, Kif2A and Dda3 is regulated in mitosis

Dda3 levels have been shown to be elevated in mitosis [17]
leading us to investigate whether ATIP3-Dda3 interaction
may also be regulated in mitosis. Co-immunoprecipitation
studies performed in synchronized MCF-7 cells expressing
GFP-ATIP3 indeed revealed that the interaction between
ATIP3 and Dda3 is increased in mitosis (Fig. 3g). Import-
antly, Kif2A binding to GFP-ATIP3 was also markedly
increased in synchronized cells although Kif2A levels
remained unchanged (Fig. 3g), which further supports the
notion that Dda3 is essential to the ATIP3-Kif2A complex.
Data showing Dda3 hyperphosphorylation in mitosis [38]
prompted us to examine whether the interaction between
ATIP3, Dda3 and Kif2A may be regulated by phosphoryla-
tion. Treatment with lambda phosphatase prior to immuno-
precipitation with GFP-ATIP3 totally abrogated both Dda3-
and Kif2A-binding to GFP-ATIP3 (Fig. S4A), indicating
that protein phosphorylation is required for ATIP3-Dda3-
Kif2A interaction.

Aurora kinase A plays a pivotal role in the ATIP3 phenotype

Mitosis is tightly regulated by mitotic kinases among which
Aurora kinase A (Aurora A), that is localized to the poles
of the spindle and whose expression is markedly increased
in G2/M. Aurora A has been shown to phosphorylate both
Dda3 [18, 38] and Kif2A [19] and to decrease the recruit-
ment and microtubule-depolymerizing activity of Kif2A at
the spindle poles [19]. We thus investigated whether Aurora
A may be a master kinase regulating ATIP3-Dda3-Kif2A
interaction.

Treatment with Aurora A kinase inhibitor MLN8054
impaired both ATIP3-Kif2A and ATIP3-Dda3 interactions
(Fig. 4a), indicating that Aurora A kinase activity is required
for ATIP3 interaction with Kif2a and Dda3. Aurora A
depletion by siRNA also markedly decreased ATIP3-Kif2A
interaction (Fig. S4B). Co-immunoprecipitation studies
revealed that Aurora A binds to GFP-ATIP3 (Fig. S4C). Of
note, ATIP3/Aurora A complexes were not always clearly



531 detectable, suggesting that this interaction may be weak and/
532 or transient.

533 In addition to disrupting the interaction of ATIP3 with
534 Kif2A and Dda3, Aurora A inactivation by silencing or
535 pharmacological inhibition mimics the phenotype of
536 ATIP3 depletion regarding Kif2A recruitment to the pole

and regulation of spindle size (Fig. S4D, S4E). This led us
to investigate whether Aurora A itself may be regulated by
ATIP3. Immunofluorescence analyses revealed that ATIP3
silencing decreases Aurora A fluorescence intensity at
spindle microtubules and poles (Figs. 4b, S4F), with no sig-
nificant change in total protein levels detected by western

537
538
539
540
541
542

Fig. 3 ATIP3-Kif2A interaction involves Dda3. **a** Left panel: Representative spinning-disk confocal live-cell images of HeLa cells in metaphase, expressing Kif2A-GFP and co-stained with SiR-DNA. Red circle indicates the bleaching area used for fluorescence recovery after photobleaching (FRAP). Scale bar, 5 μ m. Time shown in seconds. Right panel: FRAP data points represent means obtained from 28 control cells (siC) and 21 siATIP3-transfected cells (siA), collected from 3 independent experiments. The mean values of double normalized pixel intensities were plotted as a function of time and single exponential curves were fitted ($R^2 > 0.99$). Kif2A-GFP fluorescence was recovered to 89% in control cells and to 86% in siATIP3-transfected cells. The half-lives of Kif2A-GFP fluorescence recovery were calculated for control (11.62 s) and siATIP3-transfected cells (11.6 s). Error bars represent standard deviation. Representative immunoblotting data obtained from the indicated total cell extracts used in FRAP experiment is shown below the curves. **b** Left panel: HeLa cells were transfected with control (siC), ATIP3-specific (siA) and/or Dda3-specific (siD) siRNA as indicated and analyzed by immunoblotting with anti-MTUS1 (ATIP3), anti-Kif2A and anti-Dda3 antibodies. Middle panel: Immunofluorescence imaging of HeLa cells transfected as in left panel, then fixed and stained with anti-Kif2A (green) antibodies and DAPI (blue). Scale bar, 10 μ m. Right panel: Quantification of Kif2A fluorescence intensity at the poles as in Fig. 2b and quantification of spindle length as in Fig. 1b. Number of poles (for Kif2A staining) and cells (for spindle measurement) analyzed is under brackets. $**p < 0.01$, $***p < 0.001$. **c** Immunofluorescence imaging of HeLa cells transfected with control (siC) or ATIP3-specific (siA) siRNA, then fixed and stained with anti-Dda3 antibodies (magenta) and DAPI (blue). Scale bar, 10 μ m. Dda3 fluorescence intensity at the poles was measured using ImageJ software. Lower panel: Quantification of maximal Dda3 intensity in metaphase HeLa cells. Number of poles analyzed is under brackets. $***p < 0.001$. **d** Immunofluorescence imaging of MCF-7 cells stably expressing GFP or GFP-ATIP3 as indicated. Cells were fixed and stained with anti-GFP (green), anti-Dda3 (magenta) antibodies and DAPI (blue). Scale bar, 10 μ m. Lower panel: Dda3 fluorescence intensity at the poles was analyzed and quantified as in **c**. Number of poles analyzed is under brackets. $*p < 0.05$. **e** MCF-7 cells were transfected with GFP-ATIP3 or GFP and immunoprecipitation was performed using anti-GFP magnetic beads. Western blots were probed with anti-Dda3 and anti-GFP antibodies. **f** MCF-7 cells were transfected for 24 h with GFP-ATIP3 or GFP after transfection for 48 h with control (siC), Kif2A-specific (siK) or Dda3-specific (siD) siRNA, and immunoprecipitation was performed using anti-GFP magnetic beads. Western blots were probed with anti-Kif2A, anti-Dda3 and anti-GFP antibodies. Green asterisks indicate cleavage products of GFP-ATIP3. **g** MCF-7 cells were transfected with GFP-ATIP3 or GFP and left asynchronous (AS) or synchronized in mitosis (M). Immunoprecipitation was performed using anti-GFP antibodies. Blots were probed with anti-Dda3, anti-Kif2A, anti-GFP and anti-PhosphoH3 antibodies. Red asterisks indicate cleavage products of GFP-ATIP3

blot (Fig. 4b). Fluorescence intensity of the phosphorylated (Thr288) active form of the kinase was also reduced upon ATIP3 depletion (Fig. 4b), suggesting that ATIP3 contributes to maintaining an active pool of Aurora A at the poles of the mitotic spindle.

As shown in Fig. 4c, expression of RNAi-resistant GFP-ATIP3 into ATIP3-depleted cells was able to fully restore Aurora A fluorescence intensity at the spindle poles. Importantly, ATIP3-deletion mutants delCN and delCN2, that do not interact with Kif2A, were also able to rescue

the phenotype, indicating that ATIP3-mediated control of Aurora targeting to spindle poles is independent of the ATIP3/Kif2A complex.

We next examined the possibility that Aurora kinase A activity may be involved in the ATIP3 phenotype. To investigate whether the short spindle phenotype induced by ATIP3 depletion may be due to decreased Aurora A kinase activity at the poles, we ectopically expressed a GFP-Aurora A construct (GFP-AurA), or kinase-dead mutant (GFP-AurA-KD) in ATIP3-silenced cells and analyzed mitotic cells. As shown in Fig. 4d, active GFP-AurA expressed at moderate levels in ATIP3 deficient cells was able to restore a correct mitotic spindle size whereas the kinase dead GFP-AurA-KD mutant remained inefficient. Expression of GFP-AurA construct, but not the kinase dead GFP-AurA-KD mutant, also reverted the effects of ATIP3 silencing on Kif2A fluorescence intensities at the poles (Fig. 4e). Together, these results demonstrate that Aurora A kinase activity rescues mitotic spindle defects induced by ATIP3 deficiency, and highlight the central role of Aurora A in the control of metaphase spindle length by ATIP3.

Discussion

Tight control of mitotic spindle length during metaphase is essential to ensure correct cell division. Results presented here indicate that microtubule-associated protein ATIP3 controls metaphase spindle length by interacting with the microtubule depolymerizing kinesin Kif2A to negatively regulate its association with spindle poles. ATIP3 depletion causes increased Kif2A targeting to the poles, reduced poleward microtubule flux and shorter spindle size. Increased accumulation of Kif2A on spindle poles, and subsequent excessive depolymerization of spindle microtubule minus ends, may disrupt the balance between microtubule polymerization at kinetochores and depolymerization at spindle poles in metaphase, thereby leading to mild changes in poleward microtubule flux. Moderate negative regulation of microtubule flux observed upon ATIP3 depletion may also be due to its negative effect on Aurora kinase A, which was shown to regulate poleward flux via TPX2 and CLASP1 [13].

We show here by fluorescence recovery after photobleaching (FRAP) analyses that the binding of Kif2A on spindle poles is dynamic. Cytosolic pools of GFP-Kif2A were found to exchange in and out of spindle poles with half-recovery time around 10 s, which is a little faster than for other spindle pole-associated proteins such as NuMA [37]. Of note, ATIP3 silencing has no significant effect on Kif2A turnover at the poles, ruling out the hypothesis that ATIP3 may regulate the dynamic exchange between cytosolic and spindle pole pools of Kif2A proteins. The effect of ATIP3

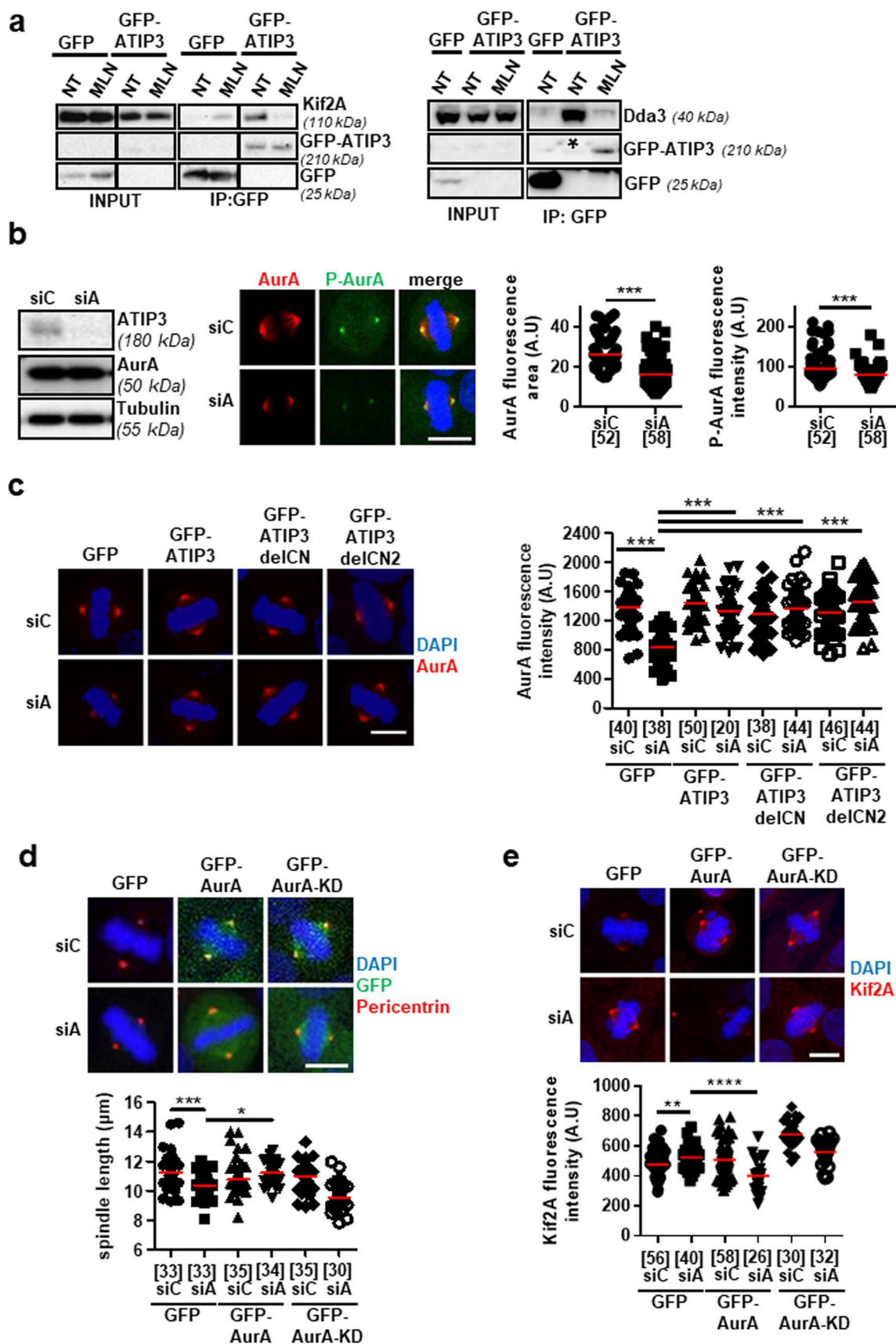


Fig. 4 Aurora kinase A plays a pivotal role in the ATIP3 phenotype. **a** MCF-7 cells were transfected with GFP-ATIP3 or GFP, then treated with 500 nM MLN8054 (MLN) (s1100, Selleckchem) or vehicle (NT) for 30 min at 37 °C, and immunoprecipitation was performed using anti-GFP antibodies. Blots were probed with anti-GFP antibodies and anti-Kif2A (left panel) or anti-Dda3 (right panel) antibodies. A black star indicates weakly detectable immunoprecipitated GFP-ATIP3. **b** Left panel: HeLa cells were transfected with control (siC) or ATIP3-specific (siA) siRNA as indicated. Immunoblotting was performed using anti-MTUS1 (ATIP3), anti-Aurora kinase A (AurA) and anti-tubulin antibodies, and indicates that ATIP3-silencing does not modify total expression levels of Aurora A. Middle panel: cells were fixed and stained with anti-Aurora A (AurA, red), anti-phospho-Aurora A (P-AurA, green) antibodies and DAPI (blue). Scale bar, 10 μm. Right panels: Quantification of the area occupied by total Aurora A fluorescence on spindles and poles, measured with ImageJ software. Phospho-Aurora A maximal fluorescence intensity at the poles was measured and quantified as in **b**. Number of poles analyzed is under brackets. *** $p < 0.001$. **c** Immunofluorescence imaging of HeLa cells transfected with control (siC) or ATIP3-specific (siA) siRNA for 48 h and then with GFP, GFP-ATIP3 or deletion mutants GFP-ATIP3delCN and GFP-ATIP3delCN2 for 24 h as indicated. Cells were fixed and stained with anti-Aurora A (AurA, red) antibodies and DAPI (blue). Scale bar, 10 μm. Right panel: quantification of Aurora A kinase fluorescence intensity as in **b**. Number of poles analyzed is under brackets. *** $p < 0.001$. **d** Immunofluorescence imaging of HeLa cells transfected with control (siC) or ATIP3-specific (siA) siRNA for 48 h and then with GFP, GFP-AurA or GFP-AurA-KD constructs for 24 h as indicated. Cells were fixed and stained with anti-GFP (green), anti-pericentrin (red) antibodies and DAPI (blue). Note that all GFP-fusion constructs are expressed at similar levels. Right panel: Quantification of pole-to-pole distance. Number of cells analyzed is under brackets. * $p < 0.05$, *** $p < 0.001$. **e** Immunofluorescence imaging of HeLa cells transfected as in **d**, then fixed and stained with anti-Kif2A (red) antibody and DAPI (blue). Right panel: Quantification of Kif2A intensity at poles as in **b**. Number of poles analyzed is under brackets. ** $p < 0.01$, *** $p < 0.001$

rather involves Dda3, a microtubule-associated protein that binds Kif2A and facilitates its recruitment to the poles [17]. As for Kif2A, ATIP3 depletion increases Dda3 accumulation on the poles. Dda3 silencing in ATIP3-deficient cells rescues the phenotype and restores basal levels of Kif2A fluorescence intensity on the poles as well as a correct size of the spindle. These findings strongly suggest that Dda3 contributes to ATIP3 effects on spindle length by regulating Kif2A recruitment to the poles. While ATIP3 regulates both Kif2A and Dda3 targeting to the poles, silencing of either Kif2A or Dda3 has no effect on ATIP3 localization, suggesting that ATIP3 is upstream of Kif2A/Dda3 and orchestrates the targeting of both proteins to the poles to control spindle length. ATIP3 interacts with Kif2A and Dda3 in a molecular complex that is increased in mitosis and requires phosphorylation by the mitotic kinase Aurora A. In return, ATIP3 is necessary to maintain an active pool of Aurora A at spindle poles, indicating a positive regulatory loop between Aurora A and ATIP3.

In the absence of ATIP3, Aurora A levels at spindle poles are decreased whereas those of Kif2A and Dda3 are increased. Expression of GFP-Aurora A kinase—but not a

kinase-dead mutant—in ATIP3-depleted cells restored basal levels of Kif2A localized at the poles as well as a correct spindle size, confirming the requirement of Aurora kinase activity in the mitotic effects of ATIP3. Together these studies favor a model by which ATIP3 regulates the localization of active Aurora kinase A during mitosis to limit Kif2A recruitment to the poles and control spindle length.

The negative regulation of Kif2A accumulation at spindle poles during metaphase is essential to prevent excessive depolymerization of microtubule minus ends that may lead to mitotic abnormalities. Besides ATIP3, other negative regulators of the Dda3/Kif2A complex have been reported. Mdp3 (microtubule-associated protein 7 domain-containing 3) forms a complex with Dda3 and Kif2A in mitosis and counteracts Dda3-mediated Kif2A recruitment to the pole [39]. Another Dda3 partner, the E3 ubiquitin ligase ASB7 (Cullin 5-interacting suppressor of cytokine signaling box 7) was shown to degrade Dda3 through the ubiquitin–proteasome degradation pathway, thereby reducing Kif2A recruitment to the pole [40]. Our data reveal a novel mechanism for negative regulation of Kif2A/Dda3 complex recruitment to the poles, which involves Aurora kinase A and its reciprocal regulation with ATIP3. Of note, ATIP3 weakly interacts with Aurora A and its amino acid sequence presents several potential Aurora A phosphorylation sites, raising the possibility that ATIP3 may also be a substrate of Aurora A. TPX2, a well-known substrate and regulator of Aurora A, also interacts with Kif2A [13] and its phosphorylation by Aurora A contributes to the regulation of poleward microtubule flux and spindle size [13, 22]. Future studies should investigate potential involvement of TPX2 in the ATIP3 phenotype.

In conclusion, results presented here provide the first evidence for the role of Aurora kinase A in the formation of a molecular complex comprising ATIP3, Kif2A and Dda3, highlighting the pivotal role of ATIP3 and Aurora A kinase cross-regulation on spindle length. This study extends our knowledge on the control of the mitotic spindle size in metaphase.

Acknowledgements We thank Dr. Sylvie RODRIGUES-FERREIRA (Inovation SAS, Paris, France) for helpful discussion. We are grateful to Dr Jamel CHELLY (Institut de Génétique et de Biologie Moléculaire et Cellulaire, Strasbourg, France) for the kind gift of Kif2A-GFP construct and Dr Stephan GELEY (Innsbruck Medical University) for U2OS-mEOS-tubulin cells. We wish to thank Dr Vasily OGRYZKO and Aline VOUILLON (Proteomics Platform of the Gustave Roussy Cancer Campus, Villejuif, France) and Fred LEEUW and Corinne LAPLACE (Plate-forme d'Imagerie et Cytométrie of the Gustave Roussy Cancer Campus, UMS 23/3655, Villejuif, France) for technical assistance and helpful discussion.

Funding This work was supported by the Inserm, the CNRS, the Ligue Nationale Contre le Cancer (Grant no. LNCC94s), the Institut Gustave Roussy, the Labex LERMIT, the GEFLUC association, the Fonds de Dotation Agnès b., the Fondation Janssen Horizon, AG2R

679 La Mondiale, the associations Odyssea and Prolific (grants to C.N.), by
680 the “Région Ile-de-France” and Fondation pour la Recherche Médicale
681 (grants to D.L.), by grants from Taxe d’apprentissage TA2015 and
682 TA2018 (University Paris-Saclay, France) (grants to A.N) and grants
683 from Lundbeck Foundation (R215-2015-4081) and Danish Cancer
684 Society Research Council (KBVU—R146-A9322) (grants to MB) and
685 Fondation ARC pour la Recherche sur le Cancer.

686 Compliance with ethical standards

687 **Conflict of interest** The authors declare that they have no conflict of
688 interest.

689 References

- 690 1. Dumont S, Mitchison TJ (2009) Force and length in the mitotic
691 spindle. *Curr Biol* 19:R749–R761. <https://doi.org/10.1016/j.cub.2009.07.028>
- 692 2. Goshima G, Scholey JM (2010) Control of mitotic spin-
693 dle length. *Annu Rev Cell Dev Biol* 26:21–57. <https://doi.org/10.1146/annurev-cellbio-100109-104006>
- 694 3. Prosser SL, Pelletier L (2017) Mitotic spindle assembly in animal
695 cells: a fine balancing act. *Nat Rev Mol Cell Biol* 18:187–
696 201. <https://doi.org/10.1038/nrm.2016.162>
- 697 4. Mitchison TJ (1989) Polewards microtubule flux in the mitotic
698 spindle: evidence from photoactivation of fluorescence. *J Cell Biol* 109:637–652
- 699 5. Mitchison TJ, Salmon ED (1992) Poleward kinetochore fiber
700 movement occurs during both metaphase and anaphase-A in
701 newt lung cell mitosis. *J Cell Biol* 119:569–582
- 702 6. Ganem NJ, Compton DA (2006) Functional roles of poleward
703 microtubule flux during mitosis. *Cell Cycle* 5:481–485. <https://doi.org/10.4161/cc.5.5.2519>
- 704 7. Goshima G, Wollman R, Stuurman N et al (2005) Length control
705 of the metaphase spindle. *Curr Biol* 15:1979–1988. <https://doi.org/10.1016/j.cub.2005.09.054>
- 706 8. Tillement V, Remy M-H, Raynaud-Messina B et al (2009) Spin-
707 dle assembly defects leading to the formation of a monopolar
708 mitotic apparatus. *Biol Cell* 101:1–11. <https://doi.org/10.1042/BC20070162>
- 709 9. Young S, Besson S, Welburn JPI (2014) Length-dependent anisotropic
710 scaling of spindle shape. *Biol Open* 3:1217–1223. <https://doi.org/10.1242/bio.201410363>
- 711 10. Gaetz J, Kapoor TM (2004) Dynein/dynactin regulate meta-
712 phase spindle length by targeting depolymerizing activities to
713 spindle poles. *J Cell Biol* 166:465–471. <https://doi.org/10.1083/jcb.200404015>
- 714 11. Ganem NJ, Upton K, Compton DA (2005) Efficient mitosis
715 in human cells lacking poleward microtubule flux. *Curr Biol* 15:1827–1832. <https://doi.org/10.1016/j.cub.2005.08.065>
- 716 12. Rath U, Rogers GC, Tan D et al (2009) The Drosophila kine-
717 sin-13, KLP59D, impacts Pacman- and Flux-based chromo-
718 some movement. *Mol Biol Cell* 20:4696–4705. <https://doi.org/10.1091/mbc.e09-07-0557>
- 719 13. Fu J, Bian M, Xin G et al (2015) TPX2 phosphorylation main-
720 tains metaphase spindle length by regulating microtubule flux. *J Cell Biol* 210:373–383. <https://doi.org/10.1083/jcb.201412109>
- 721 14. Manning AL, Ganem NJ, Bakhom SF et al (2007) The kine-
722 sin-13 proteins Kif2a, Kif2b, and Kif2c/MCAK have distinct
723 roles during mitosis in human cells. *Mol Biol Cell* 18:2970–
724 2979. <https://doi.org/10.1091/mbc.E07-02-0110>

- 736 15. Desai A, Verma S, Mitchison TJ, Walczak CE (1999) Kin I kine-
737 sins are microtubule-destabilizing enzymes. *Cell* 96:69–78. [https://doi.org/10.1016/S0092-8674\(00\)80960-5](https://doi.org/10.1016/S0092-8674(00)80960-5)
- 738 16. Cameron LA, Yang G, Cimini D et al (2006) Kinesin 5-independ-
739 ent poleward flux of kinetochore microtubules in PtK1 cells. *J Cell Biol* 173:173–179. <https://doi.org/10.1083/jcb.200601075>
- 740 17. Jang C-Y, Wong J, Coppinger JA et al (2008) DDA3 recruits
741 microtubule depolymerase Kif2a to spindle poles and controls
742 spindle dynamics and mitotic chromosome movement. *J Cell Biol* 181:255–267. <https://doi.org/10.1083/jcb.200711032>
- 743 18. Jang C-Y, Coppinger JA, Yates JR, Fang G (2011) Mitotic
744 kinases regulate MT-polymerizing/MT-bundling activity of
745 DDA3. *Biochem Biophys Res Commun* 408:174–179. <https://doi.org/10.1016/j.bbrc.2011.04.004>
- 746 19. Jang C-Y, Coppinger JA, Seki A et al (2009) Plk1 and Aurora
747 A regulate the depolymerase activity and the cellular localiza-
748 tion of Kif2a. *J Cell Sci* 122:1334–1341. <https://doi.org/10.1242/jcs.044321>
- 749 20. Barr AR, Gergely F (2007) Aurora-A: the maker and breaker of
750 spindle poles. *J Cell Sci* 120:2987–2996. <https://doi.org/10.1242/jcs.013136>
- 751 21. Magnaghi-Jaulin L, Eot-Houllier G, Gallaud E, Giet R (2019)
752 Aurora A protein kinase: to the centrosome and beyond. *Biomol-ecules*. <https://doi.org/10.3390/biom9010028>
- 753 22. Bird AW, Hyman AA (2008) Building a spindle of the correct
754 length in human cells requires the interaction between TPX2
755 and Aurora A. *J Cell Biol* 182:289–300. <https://doi.org/10.1083/jcb.200802005>
- 756 23. Rodrigues-Ferreira S, Di Tommaso A, Dimitrov A et al (2009)
757 8p22 MTUS1 gene product ATIP3 is a novel anti-mitotic protein
758 underexpressed in invasive breast carcinoma of poor prognosis.
759 *PLoS ONE* 4:e7239. <https://doi.org/10.1371/journal.pone.0007239>
- 760 24. Molina A, Velot L, Ghouinem L et al (2013) ATIP3, a novel
761 prognostic marker of breast cancer patient survival, limits can-
762 cer cell migration and slows metastatic progression by regulating
763 microtubule dynamics. *Cancer Res* 73:2905–2915. <https://doi.org/10.1158/0008-5472.CAN-12-3565>
- 764 25. Velot L, Molina A, Rodrigues-Ferreira S et al (2015) Negative
765 regulation of EB1 turnover at microtubule plus ends by inter-
766 action with microtubule-associated protein ATIP3. *Oncotarget* 6:43557–43570. <https://doi.org/10.18632/oncotarget.6196>
- 767 26. Nehlig A, Molina A, Rodrigues-Ferreira S et al (2017) Regulation
768 of end-binding protein EB1 in the control of microtubule dynam-
769 ics. *Cell Mol Life Sci* 74:2381–2393. <https://doi.org/10.1007/s00018-017-2476-2>
- 770 27. Rodrigues-Ferreira S, Nehlig A, Moindjie H et al (2019) Improv-
771 ing breast cancer sensitivity to paclitaxel by increasing aneu-
772 ploidy. *Proc Natl Acad Sci USA* 116:23691–23697. <https://doi.org/10.1073/pnas.1910824116>
- 773 28. Meraldi P, Honda R, Nigg EA (2002) Aurora-A overexpression
774 reveals tetraploidization as a major route to centrosome amplifica-
775 tion in p53^{-/-} cells. *EMBO J* 21:483–492
- 776 29. Rannou Y, Troadec M-B, Petretti C et al (2008) Localization of
777 aurora A and aurora B kinases during interphase: role of the N-ter-
778 minal domain. *Cell Cycle* 7:3012–3020. <https://doi.org/10.4161/cc.7.19.6718>
- 779 30. Courtheoux T, Diallo A, Damodaran AP et al (2018) Aurora A
780 kinase activity is required to maintain an active spindle assembly
781 checkpoint during prometaphase. *J Cell Sci* 131:jcs191353. <https://doi.org/10.1242/jcs.191353>
- 782 31. Pouillet P, Carpentier S, Barillot E (2007) myProMS, a web server
783 for management and validation of mass spectrometry-based pro-
784 teomic data. *Proteomics* 7:2553–2556. <https://doi.org/10.1002/pmic.200600784>

801 32. Valot B, Langella O, Nano E, Zivy M (2011) MassChroQ: a
 802 versatile tool for mass spectrometry quantification. *Proteomics*
 803 11:3572–3577. <https://doi.org/10.1002/pmic.201100120>
 804 33. Kowal J, Arras G, Colombo M et al (2016) Proteomic compari-
 805 son defines novel markers to characterize heterogeneous popula-
 806 tions of extracellular vesicle subtypes. *Proc Natl Acad Sci USA*
 807 113:E968–E977. <https://doi.org/10.1073/pnas.1521230113>
 808 34. Vizcaíno JA, Csordas A, del-Toro N et al (2016) 2016 update
 809 of the PRIDE database and its related tools. *Nucleic Acids Res*
 810 44:D447–D456. <https://doi.org/10.1093/nar/gkv1145>
 811 35. Wandke C, Barisic M, Sigl R et al (2012) Human chromokine-
 812 sins promote chromosome congression and spindle microtubule
 813 dynamics during mitosis. *J Cell Biol* 198:847–863. <https://doi.org/10.1083/jcb.201110060>
 814 36. Pereira AJ, Maiato H (2010) Improved kymography tools and its
 815 applications to mitosis. *Methods San Diego Calif* 51:214–219.
 816 <https://doi.org/10.1016/j.ymeth.2010.01.016>
 817 37. Stenoien DL, Sen S, Mancini MA, Brinkley BR (2003) Dynamic
 818 association of a tumor amplified kinase, Aurora-A, with the
 819 centrosome and mitotic spindle. *Cell Motil Cytoskelet* 55:134–
 820 146. <https://doi.org/10.1002/cm.10120>
 821 38. Jang C-Y, Coppinger JA, Yates JR, Fang G (2010) Phospho-regu-
 822 lation of DDA3 function in mitosis. *Biochem Biophys Res Comm-*
 823 *mun* 393:259–263. <https://doi.org/10.1016/j.bbrc.2010.01.115>
 824 39. Kwon HJ, Park JE, Song H, Jang C-Y (2016) DDA3 and Mdp3
 825 modulate Kif2a recruitment onto the mitotic spindle to control
 826 minus-end spindle dynamics. *J Cell Sci* 129:2719–2725. <https://doi.org/10.1242/jcs.180109>
 827 40. Uematsu K, Okumura F, Tonogai S et al (2016) ASB7 regulates
 828 spindle dynamics and genome integrity by targeting DDA3 for
 829 proteasomal degradation. *J Cell Biol* 215:95–106. <https://doi.org/10.1083/jcb.201603062>
 830
 831
 832
 833 **Publisher's Note** Springer Nature remains neutral with regard to
 834 jurisdictional claims in published maps and institutional affiliations.
 835

Author Proof

UNCORRECTED PROOF

Journal:	18
Article:	3614

Author Query Form

Please ensure you fill out your response to the queries raised below and return this form along with your corrections

Dear Author

During the process of typesetting your article, the following queries have arisen. Please check your typeset proof carefully against the queries listed below and mark the necessary changes either directly on the proof/online grid or in the 'Author's response' area provided below

Query	Details Required	Author's Response
AQ1	Author details: Kindly check and confirm whether the corresponding author is correctly identified.	
AQ2	Kindly check and confirm the organization name in affiliation 1.	
AQ3	Please confirm all the section headings are correctly identified.	
AQ4	Kindly check and confirm the inserted grant number (LNCC94) and funder name 'Fondation ARC pour la Recherche sur le Cancer' in funding statement.	
AQ5	Kindly check and confirm the page number for the reference [30].	

Author Proof